Local structural motifs and extended-range order in liquid and solid ammonia under pressure

M. Guthrie, C. A. Tulk, J. Molaison, and A. M. dos Santos

Phys. Rev. B **85**, 184205 — Published 14 May 2012

DOI: 10.1103/PhysRevB.85.184205

Local structural motifs and extended-range order in liquid and solid ammonia under pressure

M. Guthrie[1], C.A. Tulk[2], J. Molaison[2] & A.M. dos Santos[2]

[1] *Geophysical Laboratory, Carnegie Institution of Washington, Washington, DC, USA.*

[2] *Spallation Neutron Source, Oak Ridge National Laboratory, Oak Ridge, TN, USA.*

Neutron-diffraction measurements of the local structure in deuterated ammonia have been conducted up to pressures of 2.1 GPa and ambient temperature. Total pair-distribution functions, determined by Fourier analysis of the static structure factor, are used to examine the structural changes from the first neighbors to extended ranges of ~30 Å in both the liquid and solid state. In the proton-disordered crystalline phase III, the first coordination shell is almost identical to that of the higher pressure, ordered phase IV. The H-bond correlation is observed as a distinct shoulder at 2.5 Å. Similar local structure is seen in the liquid at a pressure just below freezing and, in particular, a pronounced H-bond correlation is observed in the liquid across the pressure range studied. A substantial increase in the ordering length scale of the liquid is observed at high pressure with correlations extending to at least 25 Å compared to ~12 Å at ambient. The decay of the primary oscillations in the extended range is exponential and well described by a simple-liquid model implying that, despite persistent H-bonding, packing considerations become the dominant structural driver as density increases.

I. INTRODUCTION

With annual world-wide production totaling 130 million metric tons (2009 data[1]), ammonia NH_3 is one of the most abundantly produced inorganic chemicals with the associated energy cost of production

estimated to account for over 1% of the total of all man-made power[2]. While the most prolific use of ammonia is for the production of agricultural fertilizers[2], it could also have a potential impact on our energy landscape as a carbon-free fuel source[3].

Improvements in the efficiencies of production and use of ammonia depend on a detailed knowledge of its inter-molecular structure and interactions. Of particular importance are studies of the chemically active liquid state. The response of structure to increased pressure provides a stringent test of theoretical potentials, which are the key to molecular-level modeling of chemical and physical properties.

Ammonia shares some similarities with H_2O in that it solidifies into a series of H-bonded "molecular ices", at least two of which exhibit orientational disorder of their molecules[4,5]. Of the three solid phases I, II and III on the liquidus up to at least 20 GPa[6] only the lowest pressure phase I (found on freezing below ~0.3 GPa) is ordered[7]. The phase diagram in Fig 1 shows the thermodynamic relations between these phases and the higher pressure, ordered, phase IV.

Orientational disorder (either dynamic or static) can mask many local structural details obtained by conventional crystallographic analysis as the intensities of Bragg peaks only provide information on structure that is both temporally and spatially averaged. For this reason, our understanding of the disordered phases II and III have, so far, relied heavily on analogies with the structure of ordered phase I. For this phase, neutron diffraction studies (of deuterated ammonia, ND_3) have given us a clear picture of the details of the local structure. The nitrogen atoms in phase I adopt a pseudo-fcc arrangement, with the first coordination shell containing 6 H-bonded neighbors at an N-N distance of 3.375 Å and 6 non-bonded neighbors at a greater distance of 3.940 Å (at a temperature of 180 K[7]). This structural arrangement is shown in Fig 2.

The disordered solid phase III is found on the liquidus at pressures above 0.7 GPa up to at least 20 GPa[6]. Correspondingly, the local structural motifs found in phase III may yield insights into the high-pressure liquid phase. Few structural measurements have been conducted on phase III, although x-ray diffraction data recorded at 1.28 GPa[4] revealed the perfect face-centered cubic symmetry (space group $Fm\bar{3}m$) of the nitrogen framework (yielding the same 12-fold local coordination as in phase I). By analogy, it was suggested that the same 6 bonded, 6 non-bonded (6B-6NB) local motif found in phase I should naturally be expected in phase III[4]. However, due to the perfect cubic symmetry, the resultant bonded and non-bonded contacts would have an equal length of 3.513 (2) Å at 1.28 GPa [4], if the N atoms are taken to be centered on the high symmetry *4a* Wyckoff sites of the $Fm\bar{3}m$ space group.

Another point of reference for phase III comes from the structure of phase IV, obtained by compressing phase III to pressures above 3.7 GPa at room temperature. This was solved from neutron powder-diffraction data in 1996[8]. In phase IV, the molecules adopt a pseudo close-packed arrangement that is approximately hexagonal. In this lower-symmetry structure, both bonded and non-bonded neighbors explore a range of N-N distances ranging from 3.17 to 3.39 Å (at 5.0 GPa)[8]. The distribution of N-N distances reveals that, although the differences between bonded and non-bonded contacts is much smaller than at ambient pressure, the non-bonded contacts remain about 0.1 Å longer on average. This observation provides circumstantial evidence that, locally, the N atoms in phase III are likely to be disordered off the 4a sites, in order to permit asymmetry between bonded and non-bonded contacts. At higher pressures, the non-bonded contacts shorten more rapidly than the bonded ones and at 24 GPa, the highest pressure where neutron diffraction has given a direct measurement, they are found to be of almost identical length[9].

While the evidence above appears to point towards a local 6B-6NB motif in all solid states up to at least 24 GPa, surprisingly, structural evidence of H-bonding in the liquid has been more controversial[10,11]. One of the earliest measurements of the local structure of the liquid at 277 K[12] and ambient pressure used x-ray diffraction to probe the radial-distribution function of the nitrogen atoms, $g_{NN}(r)$. These data revealed a first coordination shell containing 12 N atoms consistent with the close packing found in phase I. Furthermore, there is complexity in the shape of this first shell, which has a dominant peak at 3.4 Å, a pronounced shoulder at 3.7 Å and a much weaker maximum at 4.6 Å. Through analogy with phase I, the first peak and its shoulder were attributed to local H-bonded and non-H-bonded neighbors respectively (which are found at 3.4 Å and 3.9 Å in the solid). The weak peak at 4.6 Å was taken as evidence of an intermediate correlation between the first and the second N-N coordination shells that is not observed in the solid[12]. In contrast, a more recent neutron diffraction study[11] found no evidence of structure in the first N-N peak, beyond a slight asymmetry on the high-r side. In addition, a weak peak in the N-H partial at 2.25 Å is attributed to a directional H-bond, although its coordination was found to be near 2 (as opposed to the value of 3 found in the solid).

Given these ambiguities, it is useful to conduct a study of the structure in both crystalline phase III and the liquid as a function of pressure. As pressure forces the molecules to adopt an increasingly efficient packing, pressure might be reasonably expected to modify the local molecular arrangements and, thus, add to our understanding of the nature of the H-bonding including H-bond strength. In the present work, we have collected neutron total static structure factor, S(Q), data in both the liquid and solid phase III, at room temperature up to pressures of 2.1 GPa. Total pair-distribution functions, G(r) of phase III, obtained by Fourier analysis, show a local coordination shell that is closely related to that calculated for (ordered) phase IV, although their structures diverge at higher radii due to the different unit cell metric. The liquid phase responds to pressure by adopting a highly-ordered arrangement of molecules. This manifests in the diffraction patterns as a pronounced increase in the intensity of the

"principal" liquid peak, the dominant feature in the diffraction pattern at low Q (see Fig. 5) , and a greatly increased spatial extent of correlations in the G(r) compared to the ambient pressure liquid. The behavior of the differential distribution function, D(r) of the high-pressure liquid out to ~ 25 Å is found to be well described by an exponentially decaying oscillatory form, corresponding to the solution of the Ornstein-Zernike equations for simple interaction potentials[13].

II. EXPERIMENTAL METHODS AND ANALYSIS

Two cryogenic loadings[14] into toroidal anvils formed from cubic-BN were performed with samples of 99% deuterated ND_3 purchased from Sigma-Aldrich (deuterated samples were used to avoid the large incoherent scattering signal from the ^1H isotope). A VX5-PE press [15] was used to apply pressure and an encapsulating[16] null-scattering, Ti:Zr Alloy gasket was used to contain the sample. After loading, the entire anvil assembly – which is at 77K - was rapidly transferred into the press. For the first sample, an initial sealing load of 9.3 metric tons was found to result in the sample melting to the liquid state upon warming to ambient temperature. The pressure was increased on this sample, kept at room temperature, and data were collected on the high-pressure liquid immediately prior to pressure-induced freezing. After crystallization, large crystallites of phase III were observed. The resulting inadequate powder averaging prevented Rietveld analysis, and the data from this loading on phase III were not used. Subsequently, however, the hydraulic load was decreased and data were measured on the liquid at close to the room-temperature vapor pressure as practically possible.

For the second loading, a higher initial force of 16.7 metric tons was applied rapidly (< 1 min.), while the sample was still below ~100 K. This compression route ensured that the sample was maintained in solid crystalline phases both during initial compression and then during subsequent warming to room temperature. Thus, it passed through both the I-II and II-III solid-solid boundaries resulting in

reasonable powder averaging, facilitating both Rietveld and Fourier analysis on the final room temperature phase III data set. In addition, the observed peak widths show no indication of significant strain in the sample.

All diffraction data were collected using the SNAP diffractometer at the Spallation Neutron Source, Oak Ridge National Laboratory, USA. The diffractometer views a decoupled supercritical hydrogen moderator, for this experiment a bandwidth chopper was used to define a wavelength range of 0.53 to 4.07 Å. Time-of-flight spectra spanning measured in a highly pixelated Anger camera centred on a scattering angle of 48.5^{o} and spanning a total 2θ range of 45^{o} were each converted to neutron counts versus momentum transfer, Q, and summed to give a measured intensity averaged across the entire detector bank. The resulting intensities spanned a Q-range extending from 0.8 $Å^{-1}$ to 13 $Å^{-1}$.

A. Pressure and Density

In our two liquid measurements, the absence of a pressure marker caused pressure to be estimated indirectly. In the first loading (from which the liquid datasets were taken), the hydraulic load on the cell was increased in small steps until freezing was observed by the appearance of Bragg peaks in the diffraction pattern. The high-pressure liquid dataset presented here was collected on upstroke at a hydraulic load of 1 metric ton less than a subsequent dataset, which was found to contain solid phase-III. At room temperature, the melting pressure of NH_3 is known to be 1.00 (5) GPa [6,17]. Extensive experience with similar loadings shows that 1 metric ton can increase sample pressure by a maximum of ~0.1 GPa. Thus, our high-pressure liquid point is assumed to have been measured at ~0.95 GPa with an experimental uncertainty less than 0.05 GPa. The offset in freezing pressure resulting from deuteration is unknown. In liquid water, the freezing pressures of heavy water is 0.06 GPa higher than light water at room temperature[18]. Assuming a similar effect in ammonia, our best estimate of our high-pressure liquid measurement is 1.01 (5) GPa .

The low-pressure liquid dataset was measured after complete removal of hydraulic load and loosening (and then re-tightening) the breech of the press – ensuring that any remaining compression of the sample was essentially zero. Consequently, the pressure is taken to be close to the vapor pressure at room temperature of 0.79 MPa and is certainly less than ~2 MPa, which would be easily sufficient to break the partial seal on the encapsulating gasket.

The pressure-volume relationship for hydrogenous, liquid ammonia has been reported at room temperature up to 0.14 GPa by Sourirajan and Kennedy[19] and up to 0.17 GPa by Kumagai[20]. Values up to 1.0 GPa are given in the NIST Standard Reference Database. All three datasets are essentially consistent where they overlap, and the NIST values are used throughout. We have assumed that the atomic number densities for NH_3 and ND_3 at a given temperature and pressure are the same, correspondingly, our ambient pressure dataset is taken to have a density of 0.086 atomsÅ^{-3} and our 1.0 GPa dataset, a density of 0.121 atomsÅ^{-3}.

In the solid state, our refined lattice parameter for phase III of 4.884 (9) Å indicates a density of 0.1373 (7) atomsÅ^{-3}. We have not been able to find published values for the density of phase III as a function of pressure and temperature, although Von Dreele *et al*[4] give a density (of NH_3) at room temperature and 1.28 GPa of 0.131 atoms Å^{-3} .

In order to estimate the pressure corresponding to our measured phase III density, the equations of state (EOS) of the low-pressure phase I and the high-pressure phase IV, published by Fortes et al[21], were offset by a constant density so they pass through the room-temperature phase III data point of Von Dreele[4]. The pressures for the offset EOS of phases I and IV corresponding to a density of 0.1373 atoms Å^{-3} are taken as lower and upper limiting values for phase III respectively with their average giving our best estimate of the pressure of our phase III dataset: 2.1 (3) GPa.

B. Data reduction

For each of the three data sets, the total measured intensity from the sample and its container (the pressure cell), as a function of Q, was corrected by subtracting an empty cell measurement. A separate background measurement was conducted for each of the two loadings. In both cases, the recovered, deformed gasket from the sample loading was used for this data collection. Due to elastic expansion of the gasket during decompression, the anvil separation (and, correspondingly, the total intensity of the background measured from the recovered gasket) differed from the sample measurement, and it was necessary to correct for this by multiplying the background using a constant scale factor as described below.

The background-subtracted signal was then corrected for the Q-dependence of variables such as the incident flux profile, the detector efficiency and attenuation due to the cell itself by dividing by an '*in-cell*' vanadium measurement. In this measurement, a vanadium pellet with almost identical geometry to the sample was placed in a gasket inside the pressure cell in a way that mimicked the exact arrangement for the sample. In addition, a further background measurement was made of this gasket in the cell without the vanadium present. As with the sample, this background signal was scaled and then subtracted from that of the in-cell vanadium. A spherical absorption correction (the vanadium and sample volumes are approximately spherical in shape) was applied to the background corrected vanadium dataset to give a normalization function. This adaptation of standard normalization procedure on spallation neutron sources (see e.g. ATLAS manual[22]) has the added advantage of including a correction for the cell attenuation. This approach has been used previously to correct neutron diffraction data from glasses[23]. Finally, the resulting background subtracted signal from the sample was corrected for its own self attenuation (again using a spherical approximation).

In obtaining final S(Q) functions, there are, thus, two unknown scale factors: one for the background and one overall scale factor. These were well determined given the two constraints that:

(1) At high Q, the S(Q) must tend to the scattering due to the intra-molecular structure of an ammonia molecule. This constraint is well justified because crystallographic studies of the ordered crystalline phase IV show no evidence of changes in molecular geometry up to ~ 15 GPa[8,9]. The coherent intra-molecular differential scattering cross-section $\left(\frac{d\sigma}{d\Omega}\right)_{intra}$ is given by:

$$\left(\frac{d\sigma}{d\Omega}\right)_{intra} = \sum_{\alpha=1}^{m}\langle b_\alpha\rangle^2 + \sum_{\substack{\alpha,\beta=1 \\ (\alpha\neq\beta)}}^{m}\langle b_\alpha\rangle\langle b_\beta\rangle \frac{\sin Qr_{\alpha\beta}}{Qr_{\alpha\beta}} \exp\left(-\frac{\langle r_{\alpha\beta}^2\rangle Q^2}{2}\right) \qquad - \ (1)$$

The first sum on the right-hand side reflects the scattering from the *m=4* isolated nuclei, α, in a molecule and is independent of Q within the energy range of these experiments. The second term is summed across all pairs of nuclei α,β within the molecule and reflects the interference between neutrons scattered from *different* nuclei in the *same* molecule[24]. The other variables in this equation are the coherent neutron scattering lengths $\langle b_\alpha\rangle$ of nucleus, α; the separation between nuclei α and β, $r_{\alpha\beta}$; the mean square vibrational amplitude $\langle r_{\alpha\beta}^2\rangle$ of pair α,β; and, the momentum transfer, Q.

In order to compare this cross-section to the structure factor, S(Q), $\left(\frac{d\sigma}{d\Omega}\right)_{intra}$ was calculated using parameters given by Betagnolli et al[25] (also determined using room temperature data) of N-D = 1.01 Å, D-$\widehat{N}$-D=112.1°, $\langle r_{ND}^2\rangle = 0.074$Å^2 and $\langle r_{DD}^2\rangle = 0.146$Å^2. The resulting value was then normalized to give an intra-molecular $S_{intra}(Q)$ (dashed-dotted line in Fig. 5) by dividing by the self scattering term $\sum_{\alpha=1}^{m}\langle b_\alpha\rangle^2$.

(2) At Q = 0, S(Q) must tend smoothly to the thermodynamic limit $S_{therm}(0)= \rho k_B T \mathrm{K_T}$ where ρ is the density (throughout this work, atomic densities expressed as atoms$Å^3$ are used), k_B is Boltzmann's constant, T temperature and $\mathrm{K_T}$ isothermal compressibility[26]. For our datasets measured at 0.0, 1.0 and 2.1 GPa, these limits were calculated to be 0.053, 0.0267 and 0.002, respectively. The data were required to pass smoothly, without discontinuity, through a fourth-order polynomial extrapolation of the low Q (<1.6 $Å^{-1}$) part of the measured S(Q) constrained to pass through $S_{therm}(0)$.

No further correction was applied for the samples own attenuation (which is assumed negligible), or multiple scattering from the sample. In addition, no attempt was made to apply an inelastic correction to the S(Q). In the case of samples, such as ND_3, where the majority of nuclei are of comparable mass to the neutron, inelastic effects – principally the recoil of the sample nucleus in response to the collision of an incident neutron, may be substantial. However, as recently reviewed by Soper[24], there remains no clear consensus for how to apply analytical corrections for this effect for sample nuclei with masses comparable to that of the neutron itself. Furthermore, as the recoil reflects the local bonding environment, it is highly likely to be pressure dependent, especially as our measurements span a density increase of ~60% and traverse both the liquid and solid states. However, as the inelastic correction is typically a slowly varying function of Q[24], it is not expected to have a substantial effect on intermolecular structure beyond ~ 2Å. This assumption is examined further in the following section.

III. Results and Discussion

The diffraction pattern of phase III confirms the face-centered cubic symmetry and corresponding orientational disorder found by x-ray diffraction[4]. The diffraction data were fitted by Rietveld structural refinements[27,28] using a model with deuterons disordered over the *(x,x,x) 32-f* Wyckoff positions and the nitrogen atoms located at the cell origin (0,0,0). With this arrangement, the molecular D-N-D angle is constrained to the perfect tetrahedral value of 109.5^{o}, which is significantly higher than the value found in the gas phase[29] (106.7^{o}), and solid phases I[7]and IV[8] (~107.8^{o}). Correspondingly, it was expected that the deuterons may not lie exactly on the *(x,x,x)* sites. Rather than place the deuterons on lower symmetry sites, anisotropic atomic displacement parameters (ADP's) were used to quantify the total extent of the deuteron density distribution. Meanwhile, the N atom was refined with an isotropic (spherically symmetric) ADP. The resulting best fit to the data (shown in Fig. 4) exhibited very large anisotropies of the deuteron thermal motion in the direction perpendicular to the N-D bond. These are illustrated in the insert to Fig 4 and are indicative of molecular orientations that are completely disordered in the temporally and spatially averaged Bragg structure. Furthermore, the refined N-D bond length of 0.840 (10) Å is substantially shorter than that found in either phases I or IV of around 0.98 Å[7,8]. This difference could be an indication that the N atom is also offset from the origin of the unit cell and, correspondingly, is also disordered over multiple sites centered on the origin. Another observation that is consistent with this hypothesis is the large value observed for the (isotropic) displacement parameter for N of 0.058 Å^2 and the similarly large value of the component of the deuteron displacement parallel to the N-D bond of 0.066 Å. Such behavior is analogous to that found in disordered water phases Ih[30] and VII[31–33], most prominently in the latter where Bragg refinements[31–33] yield O-D bond lengths of 0.89 to 0.92 Å compared with the accepted value of 0.98 Å.

The structure described above, determined by Rietveld analysis of the crystalline Bragg peak intensities, reflects both a temporal and spatial average of the nuclear positions. Local deviations from this average manifest themselves as diffracted intensity that is distributed over the continuum of reciprocal space.

Thus, in an orientationally disordered crystal, intensity is lost from the Bragg peaks and appears in the form of delocalized, diffuse scattering. In the case of liquids, all of the coherent scattering manifests as diffuse intensity.

As described above, static structure factors, S(Q), were determined both for the liquid at pressures near ambient, at 1.0 GPa just before freezing, and for crystalline phase III at 2.1 GPa (Fig. 5). The liquid data are dominated by a single, strong 'principal'peak at low Q, whereas at higher Q, the broad form of the S(Q) matches that expected for the self scattering of the ammonia molecule. With increasing pressure, this intra-molecular geometry remains essentially unchanged, consistent with the observation that up to substantially higher pressures (in phase IV, up to at least 24 GPa) this was found to remain essentially identical to that at ambient pressure[8,9].

In contrast, the principal peak, which is sensitive to the *inter*-molecular structure, shows pronounced pressure-dependence as it shifts to higher Q while it sharpens significantly. Ricci *et al*[11] demonstrated that a pronounced peak is found in all three partial S(Q) at around 2.1 $Å^{-1}$. For our deuterated sample, we can safely assume, however, that this feature is predominantly sensitive to real-space periodicities in the N-D and D-D correlations (as detailed below, these constitute 90% of the total signal). This behavior of the first peak is consistent with an increase in the length scale of ordering and of a shortening of the first-shell, intermolecular N-D and D-D correlations as pressure increases. Ultimately, upon freezing, this scattered intensity coalesces into the Bragg peaks seen for crystalline phase III.

The S(Q) data (Fig 5) can be used to calculate a total radial distribution function G(r) for both the crystalline and liquid phases using the Fourier relationship:

$$G(r) - 1 = \frac{1}{2\pi^2 \rho r} \int_0^\infty dQQ[S(Q) - 1]\sin(Q.r) \qquad \text{- (2)}$$

The G(r) represents the probability that a nucleus is found at a distance r from another nucleus at the origin. It is normalized to the bulk atomic density ρ and, therefore, tends to 1 at high r in liquids or glasses with a finite correlation length. In the case of ammonia, where there are two distinct nuclear species present, the total G(r) in Eqn. 2 can be decomposed into a linear combination of the individual pair correlations $g_{\alpha\beta}(r)$ between these species α and β. These 'partial' g(r) are weighted by their Faber-Ziman coefficients[34], such that

$$G(r) = \sum_{\alpha=1}^{n}\sum_{\beta=1}^{n}\frac{c_\alpha c_\beta \langle b_\alpha\rangle\langle b_\beta\rangle}{\langle b\rangle^2}\left[g_{\alpha\beta}(r)\right] \quad \text{- (3)}$$

where c_α is the concentration of atomic species, α, in the material (e.g. 0.25 for N in ND_3), and $\langle b\rangle^2$ is the mean coherent scattering length ($\sum_{\alpha=1}^{n} c_\alpha\langle b_\alpha\rangle$). For ammonia, there are three such partial correlations: N-N, N-D and D-D, which each contribute 10%, 46% and 44% of the total signal respectively.

Fig 6 shows the intermolecular correlations of the total G(r) obtained directly from Fourier transform of the S(Q) data from crystalline phase III. Because these data are sensitive to the *local* structure, they provide new information that supplements that contained in the Bragg intensities. As a starting point in interpreting these data, it's useful to compare our phase III data with the known structures of the two ordered crystalline phases I and IV. Radial distribution functions for these data were calculated using the published crystal structures[7,8]. In order to correct for the density difference between our measurement of phase III and those of the published structures, the lattice parameters were scaled (using constant multiples of 1.0578 for phase IV and 0.954 for phase I) to give an equal atomic density as compared with our phase III measurement. In addition, the fractional coordinates of the deuterons were also scaled in order to retain the original molecular geometry, while the fractional coordinates of the nitrogen atoms were unchanged. In this way, the absolute N-N distances in each model are reduced or increased by the same multiple as the unit cell, but the local orientational arrangements of the molecules are kept the

same as in the original unit cell. To obtain a representative G(r) for each phase, the unit cells were replicated multiple times to yield supercells of edge size ~50Å containing ~5600 molecules each. A small, Gaussian-distributed random shift was then applied to simulate both thermal motion and the broadening effect corresponding to our finite Q-range before, finally, the G(r) were determined directly from the simulation cell using software included in the RMCProfile distribution[35]).

These calculated G(r)'s are compared with that measured for phase III in the region of the first intermolecular contacts up to 20 Å (Fig. 6). If we initially consider the first intermolecular shell of phase III (Fig 6, inset), a close match with phase IV is clear, while phase I is quite different. Although phase I has a pseudo-fcc arrangement, it differs from phase III in that the non-bonded contacts are much longer than the H-bonded N-N contacts (at 3.758 vs. 3.220 Å). In contrast, the pseudo-hcp arrangements in phase IV have a much more symmetric local environment where non-bonded contacts are on average only ~ 0.1 Å greater than bonded contacts (3.321 vs. 3.215 Å). As the G(r) averages over the angular distribution, it is not surprising that the first shell of an hcp lattice is similar to that of an fcc lattice.

Given the close similarity in local structure, one may use each individual partial $g_{\alpha\beta}(r)$ from the model phase IV (also shown in Fig 6) to interpret the total G(r) of phase III as far as the first molecular contacts. These partials are also shown in Fig. 6. It seems clear, based on inspection of the these partials, that the pronounced shoulder observed at ~2.4 Å in phase III (marked with an arrow in Fig 6, inset) is attributable to protons at the first N...D H-bond contact.

The differences between the hcp and fcc local arrangements should begin to manifest at distances comparable to the twice the average close-packed layer distance (i.e. ABC vs. ABA) of 5.4 Å. And, the G(r)'s for phases IV and III diverge near this value. As the radius increases further, the G(r) begins to reflect more closely the averaged, Bragg, structure. Beyond about 6 Å, the G(r) of phase IV is almost completely out of phase with that of phase III, reflecting the different packing: hexagonal in the former

and cubic in the latter. Meanwhile, at the highest radii, the shared cubic metric of the scaled model of phase I results in perfectly in-phase density oscillations. With this insight into the local structure in crystalline phase III, we can now make a comparison with high and low pressure liquids. If we consider first the short-range contacts, shown in the inset to Fig. 7, there are two intra-molecular peaks (the N-D at an average distance of 0.992 (13) Å and the D...D at 1.7 Å).

A property of the partial $g_{\alpha\beta}(r)$ is that the mean number of β nuclei n_{α}^{β} contained within concentric shells of radius r_1 and r_2 about an α nucleus is proportional to the integrated area of $g_{\alpha\beta}(r)$ between these same two radii and the density ρ.

$$n_{\alpha}^{\beta} = 4\pi\rho c_{\beta} \int_{r_1}^{r_2} dr r^2 g_{\alpha\beta}(r) \qquad \text{-(4)}$$

As the first N-D peak only minimally overlaps with the adjacent intra-molecular D...D peak, and with no other correlations, the $g_{ND}(r)$ partial in this region could be readily extracted by fitting with a Gaussian (which gives a good match for the measured peak shape). The coordination of D about N is exactly 3.0 at ambient pressure. However, for the liquid at 1.0 GPa and the solid at 2.1 GPa the coordination number is 3.5. The possibility that this might be the result of some reaction between the ammonia and the Ti:Zr containment was discounted as the low pressure liquid was from the same loading as the high pressure liquid, and was measured last. The most likely explanation seems to be that this reflects the sensitivity of the low-r features in G(r) to either subtle errors in the attenuation and multiple scattering due to the sample and its containment or to the (uncorrected for) inelastic scattering. The spurious structure seen in the G(r) below ~ 0.5 Å, which grows with pressure, is also evidence of this, although this artifact appears to not contribute significantly to the inter-molecular structure above ~2 GPa.

Just beyond the intra-molecular peaks, a shoulder centered on ~2.5 Å is seen in all three patterns and, based on the strong similarities between the local structure of phase IV and III, this is identified as the

first H-bond contact. Our G(r) data have insufficient resolution to separate the N-D partial in this region from the overlapping D-D peaks, but there is clearly no strong difference in the intensity of this feature from the low pressure liquid up to the solid phase III. This suggests that, contrary to the conclusion by Ricci et al[11], there is a full population of 3 protons at the H-bonded distance between neighbors in the liquid even at ambient pressure.

In order to examine the longer-range structure, it's useful to use the differential distribution function, *D(r)* where $D(r) = 4\pi\rho r[G(r) - 1]$ as the factor of *r* serves to amplify residual structure at higher radii. In Fig 7, the measured D(r) data are shown for both liquids out to 30 Å. The most striking observation from these figures is the substantial increase in the extent of spatial correlations at high *r*, relative to low pressure.

The gradual decay of oscillations in the 1.0 GPa liquid D(r) is reminiscent of that found in simple Lennard-Jones fluids, and this motivated an attempt to fit these data with a correspondingly simple model. Evan's et al [13] have calculated the solution of the Ornstein-Zernike (OZ) equations for systems interacting via pair-potentials arising from only short-range repulsive and long-range Coulomb interactions. For this simple case, the asymptotic behavior of the pair-correlations is oscillatory and subject to an exponential decay:

$$D(r) = 4\pi\rho r[G(r) - 1] = 8\pi\rho|\mathrm{A}|\exp(-a_0 r)\cos(a_1 r - \theta) \qquad \text{- (5)}$$

Here $|\mathrm{A}|$ is the amplitude, a_1 describes the primary oscillation frequency and $\xi = 1/a_0$ defines a characteristic correlation length for the liquid.

Salmon et al[36–38] have studied this 'extended-range' structure (ERS) extensively in tetrahedral glasses and liquids and observed that the functional form of Eqn. 5 describes both ionic and covalent network glasses (GeO_2 and $ZnCl_2$), remarking that the long-range decay was independent of the nature of the

local bonding[37]. Furthermore, the same asymptotic behavior is seen for systems as diverse as binary metallic liquids[39] and liquid noble gases such as Ar[40], all of which have non-directional interaction potentials.

The ERS shown in the D(r) for high-pressure liquid ammonia is also remarkably well described by the functional form of Eqn. 3 to all but the first coordination shell in r (Fig. 7A), which has additional structure imposed by both the H-bonding and the anisotropic geometry of the molecules themselves. The parameters of the OZ fit give a correlation length ξ= 6.2 Å that is comparable with the value of 5.9 Å found for liquid Ar and more than double that of ~ 3 Å found for binary metallic glasses[39]. In contrast, the value obtained for the ambient pressure liquid is only 3.4 Å, indicating that the correlation length is significantly increase in the high-pressure liquid.

In examining the long range decay of the oscillations in D(r), it's important to also consider the effect of instrumental resolution. Through the convolution theorem, the Q-space resolution function of the diffractometer propagates as a multiplicative function that also results in a gradual decay of the oscilliations measured in real space. We can measure this effect by considering the limits of real space oscillations observed for our crystalline phase III dataset. This is shown in Fig. 7B along with the modification function M(r) expected for a diffractometer with a Gaussian resolution function of width, dQ = 0.03 Å^{-1}, which is given by $M(r) = exp[-(dQr)^2/2]$ (see e.g.). We can estimate the impact of the instrumental resolution, taking dQ=0.03, by dividing by this function prior to applying the OZ fit described in the preceding paragraphs. This results in a 10% increase of the correlation length for the liquid at 1.0 GPa, ξ(1.0) = 6.8 Å, while the low pressure liquid sees little change, with ξ(0.0) increasing slightly to 3.5 Å. The net effect of this resolution correction is to enhance the difference between the low and high pressure correlation lengths, which are now almost doubled in the latter relative to the former.

Another parameter that can be taken from the OZ fits is the real-space periodicity, a_1 = 2.158 $Å^{-1}$ in the high-pressure liquid and corresponds to a separation between successive shells in the liquid, $\Lambda_{liq} = 2\pi/a_1$ =of 2.912 Å. A similar oscillatory fit to the solid phase-III D(r) yields an equivalent ERS shell separation of Λ_{sol} = 2.820 Å. This shorter value for the shell separation in the solid simply reflects its higher density relative to the liquid. Finally, the angular phases of the liquid θ_{liq} and solid θ_{sol} are rather similar at 1.38 and 1.54 radians, respectively. This contrast with the difference of approximately π found between phases III and IV suggests that the long-range packing in the high pressure liquid is similar to the cubic close-packed structure in solid phase III.

The ability of such a simple model to describe the structure of ND_3 while H-bonding is retained is striking. Furthermore, it resonates with the observations of Salmon et al[37], on network glasses and liquids, that the structural effect of densification can be viewed as a competition between intermediate range order (dictated by the nature of local bonding) and extended range structure (dictated by packing considerations) that ultimately must be won by the latter as density increases. Although liquid ammonia has no intermediate-range order, we see clear evidence of local interactions in the H-bond correlation and the local coordination environment, which looks very similar to that dictated by H-bonding in the solid phases III and IV.

These pronounced differences between the low and high-pressure liquid are also reminiscent to those reported in liquid water by Strässle et al[41]. This neutron diffraction study found that, at high pressure and temperature, the O-O partial of deuterated water resembled that of liquid Ar, while the number of H-bonds remained equal to that found at ambient conditions. This observation, together with our results and those of Salmon et al[36–39], point to the possibility of a general phenomenology observed in both dense liquids and glasses: a lowering of the significance of the local bonding schema in the bulk

structure at elevated densities. This has important consequences for theoretical attempts to predict bulk properties, such as viscosity and heat capacity, which are based on microscopic structure. It also highlights the importance of using probes, such as diffraction, which can simultaneously determine structure across a wide range of length scales.

IV. CONCLUSIONS

We have determined the static structure factors of deuterated ammonia at room temperature. These were measured in the liquid state at ambient pressure and just before freezing and in the solid phase III after freezing. By Fourier transform of these data, we have obtained total G(r) revealing the local intra and inter-molecular correlations as a function of density, which we control with pressure. Comparison with calculated G(r) of the higher pressure phase IV shows a close relation with the local structure phase of phase III. A peak corresponding to the first H-bond contact is identified from this comparison, and the same peak is also found in the liquid across the pressure range studied. Although this local bonding scheme is retained, we observe a stark increase in the extent of structural correlations in the liquid at high pressure. This suggests a cross over in the relative roles of local bonding and packing considerations, as density increases, which is identified as a somewhat general phenomenon, observed in a wide range of binary glasses and also in liquid water.

ACKNOWLEDGMENTS

This work was supported entirely by EFree, an Energy Frontier Research Center funded by the U.S. Department of Energy, Office of Science, Office of Basic Energy Sciences under Award Number DE-SC0001057. Use of the Spallation Neutron Source is supported by the Division of Scientific User Facilities, Office of Basic Energy Sciences, US Department of Energy, under contract DE-AC05-

00OR22725 with UT-Battelle, LLC.We also wish to thank Prof P S Salmon for valuable discussions and Dr. M.G. Tucker for help in preliminary experiments.

Figure Captions

Fig 1: *Structural phase diagram of pure hydrogenous ammonia. The I-II transition line and the melting line of phase I are taken from Mills et al*[42]*), the melt line of phases II and III and the III-IV transition temperature are from Ninet et al*[6]*. The II-III transition temperature appears to be not well determined: the dashed line shown is taken from Gauthier et al*[43]*, who cites a private communication With R.L. Mills. Each solid phase is labeled with its Herman-Mauguin space group (in brackets) and whether the local structure is orientationally disordered (dis) or ordered (ord).*

Fig 2: *(color online) Visualisation*[44] *of Ammonia-phase I, blue (large) spheres indicate N atoms, pink (small) spheres indicate H(D) atoms, dashed lines represent H-bonds. The figure shows the first pseudo-fcc 12-fold coordination shell of molecules about the central molecule labeled A. These neighboring molecules adopt an arrangement where 6 are H-bonded to molecule A (3 donating and 3 accepting), while the other 6 are not bonded to molecule A. The pseudo close-packed layers lie parallel to the a-b plane.*

Fig 3: *shows atomic densities for relevant states of ammonia. Open squares indicate Kumagai's low pressure densities*[20]*, the solid black line passing through these are the NIST* Standard Reference Data*. Fortes et al's Equations-of-state (EOS)*[21] *for phases I and IV (solid lines, marked) offset to pass through Von Dreele's room temperature data point at 1.28 GPa*[4]*, shown as a star. The solid horizontal line gives our experimentally measured density for phase III, with horizontal dash-dot lines showing the standard deviation. The vertical grey band indicates the corresponding estimated range of pressure for our phase III data point.*

Fig 4: *(Color online) The Rietveld fit to phase III at 2.1 GPa, circles indicate data points, the solid line passing through these is the fit and the line below these the residual. All peaks in the pattern are accounted for by the $Fm\bar{3}m$ space group. The insert shows the 67% probability contour of the deuteron thermal ellipsoids, suggesting the molecular orientations are completely disordered in the temporally and spatially averaged structure measured by the Bragg diffraction measurement.*

Fig. 5: *(Color) The S(Q) data for the room temperature liquid at ambient pressure (blue) and just below pressure-induced freezing at room temperature at 1.0 GPa (green) as well as the solid phase III at 2.1 GPa (red). These data were truncated where the S(Q) crosses a value of 1.0 (at 12.0 $Å^{-1}$) in order to minimize truncation ripples in the Fourier transforms. The weak Bragg peak in the liquid data at 3.2 $Å^{-1}$ is due to a small amount of gold loaded with the sample with the aim of providing pressure calibration, but which was found to be insensitive to the small pressure change of 1.0 GPa. Also shown by a dotted line is the expected scattering due to self scattering of the molecule, $S_{intra}(Q)$, as described in the text. The inset shows the behavior in the low-Q region.*

Fig 6: *(Color online) Shows the measured G(r) for phase III and calculated G(r) for phases I (green) and IV (red), data are shown above 2 Å reflecting the inter-molecular structure. The statistical noise in the calculated G(r) arises from the finite number of molecules in the simulation box. Also shown in gray in the lower half of the figure are the distinct partials (scaled according to their Faber-Ziman weights) that make up the total G(r) for phase IV. The inset shows the low-r part of the measured and calculated G(r) spanning the first coordination shell. The shoulder on the low r side of the main peak, marked with an arrow in the inset, corresponds to the first inter-molecular N-D correlation i.e. the H-bonded contact.*

Fig. 7: *A shows D(r) correlation functions for both liquids extending from first inter-molecular contact to 30 Å. The data for the 1.0 GPa liquid are offset by 1.0 on the y-axis for clarity. Superimposed on the 1.0*

GPa liquid data as a dashed (red) curve is a simple Ornstein-Zernike model fitted between 4.3 and 28 Å. The inset shows the G(r) data for both liquids and phase III at low r, including the two intra-molecular peaks and the first coordination shell. The H-bond correlation is marked here by an arrow. B shows r[G(r)-1] for crystalline phase III out to 120 Å the decay of the oscillations with increasing r reflects the finite dQ resolution of the instrument. The grey curve indicates the expected fall off in r-space for a diffractometer with a Gaussian resolution function of width 0.03Å^{-1}.

References

[1] *US Geological, Survey Mineral Commodities Summary* (2011), pp. 112-113.

[2] *Ullman's Encyclopedia of Industrial Chemistry* (Wiley, 2006).

[3] J.R. Bartels and M.B. Pate, *A Feasibility Study of Implementing an Ammonia Economy* (2008).

[4] R.V. Dreele and R. Hanson, Acta Crystallographica Section C: Crystal Structure **40**, 1635-1638 (1984).

[5] J. Eckert, R.L. Mills, and S.K. Satija, The Journal of Chemical Physics **81**, 6034 (1984).

[6] S. Ninet and F. Datchi, The Journal of Chemical Physics **128**, 154508 (2008).

[7] A. Hewat and C. Riekel, Acta Crystallographica **A35**, 2483-2484 (1979).

[8] J.S. Loveday, R.J. Nelmes, and W.G. Marshall, Physical Review Letters 1-4 (1996).

[9] S. Ninet, F. Datchi, S. Klotz, G. Hamel, J. Loveday, and R. Nelmes, Physical Review B **79**, 8-11 (2009).

[10] D.D. Nelson, G.T. Fraser, and W. Klemperer, Science (New York, N.Y.) **238**, 1670-4 (1987).

[11] M.A. Ricci, M. Nardone, F.P. Ricci, C. Andreani, and A.K. Soper, **102**, 7650-7655 (1995).

[12] A.. Narten, Journal of Chemical Physics **66**, 3117-3120 (1977).

[13] R. Evans, R.J.F. Leote de Carvalho, J.R. Henderson, and D.C. Hoyle, The Journal of Chemical Physics **100**, 591 (1994).

[14] J.S. Loveday and R.J. Nelmes, Physical Chemistry Chemical Physics: PCCP **10**, 937-50 (2008).

[15] S. Klotz, G. Hamel, and J. Frelat, High Pressure Research **24**, 219-223 (2004).

[16] W.G. Marshall and D.J. Francis, Journal of Applied Crystallography **35**, 122-125 (2002).

[17] T. Kume, M. Daimon, S. Sasaki, and H. Shimizu, Physical Review B **57**, 347-350 (1998).

[18] W.F.T. Pistorius, E. Rapoport, and J.B. Clark, Journal of Chemical Physics **48**, 5509-5514 (1968).

[19] S. Sourirajan and G.C. Kennedy, Journal of Geophysical Research **68**, 4149-4155 (1963).

[20] A. Kumagai and T. Toriumi, Journal of Chemical and Engineering Data **16**, 293-295 (1971).

[21] A.D. Fortes, J.P. Brodholt, I.G. Wood, and L. Vočadlo, The Journal of Chemical Physics **118**, 5987 (2003).

[22] A.K. Soper, W.S. Howells, and A.C. Hannon, *ATLAS - Analysis of Time-of-flight Diffraction Data from Liquid and Amorphous Samples* (1989), pp. RAL-89-046.

[23] J.W.E. Drewitt, P.S. Salmon, A.C. Barnes, S. Klotz, H.E. Fischer, and W. a. Crichton, Physical Review B **81**, 30-35 (2010).

[24] A.K. Soper, Molecular Physics **107**, 1667-1684 (2009).

[25] P. Chieux and H. Bertagnolli, Society 3726-3730 (1984).

[26] P.A. Egelstaff, *An Introduction to the Liquid State*, 2nd ed. (Oxford University Press, New York, 2002).

[27] A.C. Larson and R.V. Dreele, Los Alamos National Laboratory Report **LAUR 86-74**, (2000).

[28] B.H. Toby, Journal of Applied Crystallography **34**, 210-213 (2001).

[29] W.M. Haynes and D.R. Lide, editors, *Handbook of Chemistry and Physics*, 91st ed. (Internet Version, 2011).

[30] W.F. Kuhs and M.S. Lehmann, Water Science Reviews **2**, 1-65 (1986).

[31] W.F. Kuhs, J.L. Finney, C. Vettier, and D.V. Bliss, Journal of Chemical Physics **81**, 3612-3623 (1984).

[32] J.D. Jorgensen and T.G. Worlton, Journal of Chemical Physics **83**, 329-333 (1985).

[33] R.J. Nelmes, J.S. Loveday, and W.G. Marshall, Physical Review Letters 2719-2722 (1998).

[34] T.E. Faber and J.M. Ziman, Phil Mag. **11**, 153-173 (1965).

[35] M.G. Tucker, D. a Keen, M.T. Dove, A.L. Goodwin, and Q. Hui, Journal of Physics. Condensed Matter□: an Institute of Physics Journal **19**, 335218 (2007).

[36] P.S. Salmon, Journal of Physics: Condensed Matter **19**, 455208 (2007).

[37] P. Salmon, A. Barnes, R. Martin, and G. Cuello, Physical Review Letters **96**, 1-4 (2006).

[38] P.S. Salmon, Journal of Physics: Condensed Matter **18**, 11443-11469 (2006).

[39] P. Chirawatkul, A. Zeidler, P. Salmon, S. Takeda, Y. Kawakita, T. Usuki, and H. Fischer, Physical Review B **83**, (2011).

[40] J. Yarnell, M. Katz, R.G. Wenzel, and S. Koenig, Physical Review A **7**, 2130 (1973).

[41] T. Strässle, a. Saitta, Y. Godec, G. Hamel, S. Klotz, J. Loveday, and R. Nelmes, Physical Review Letters **96**, 1-4 (2006).

[42] R.L. Mills, D.H. Liebenberg, and P. Pruzan, Journal of Physical Chemistry **86**, 5219-5222 (1982).

[43] M. Gauthier, P. Pruzan, J.C. Chervin, and J.M. Besson, Physical Review B **37**, 2102-2115 (1988).

[44] K. Momma and F. Izumi, Journal of Applied Crystallography **41**, 653-658 (2008).

Figure 1 Guthrie et al, PRB

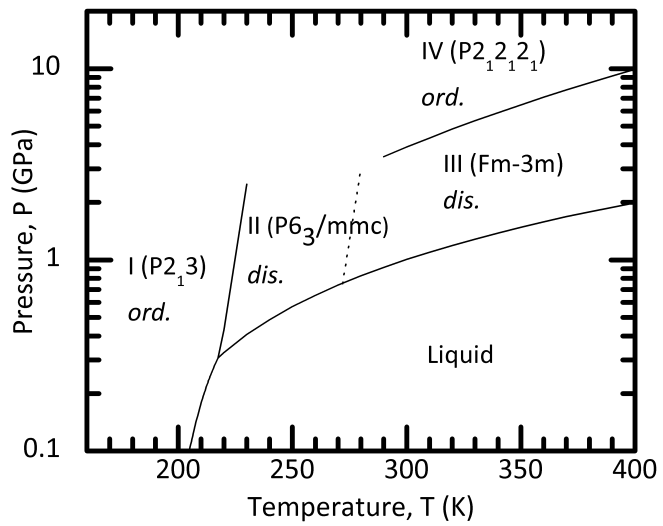

Figure 1 BMR1184B 23FEB2012

Figure 2 Guthrie et al, PRB

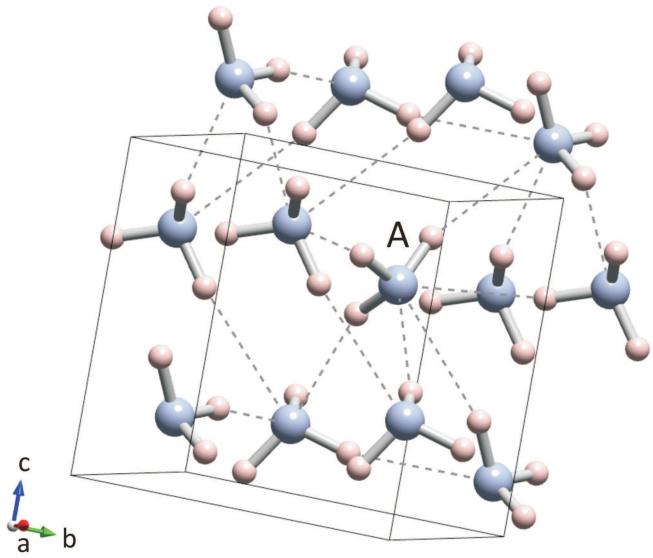

Figure 2 BMR1184B 23FEB2012

Figure 3 Guthrie et al, PRB

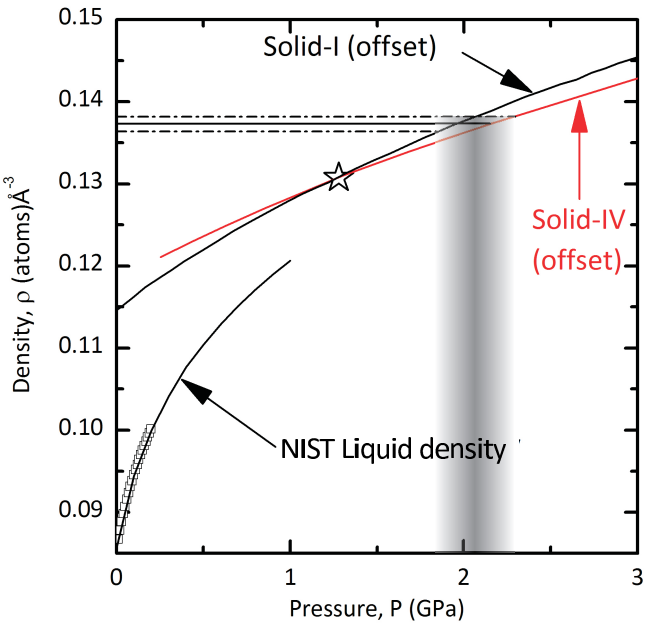

Figure 3 BMR1184B 23FEB2012

Figure 4 Guthrie et al, PRB

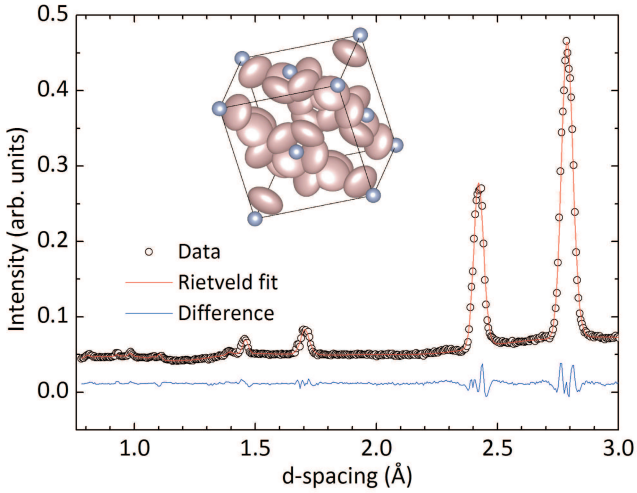

Figure 4 BMR1184B 23FEB2012

Figure 5 Guthrie et al, PRB

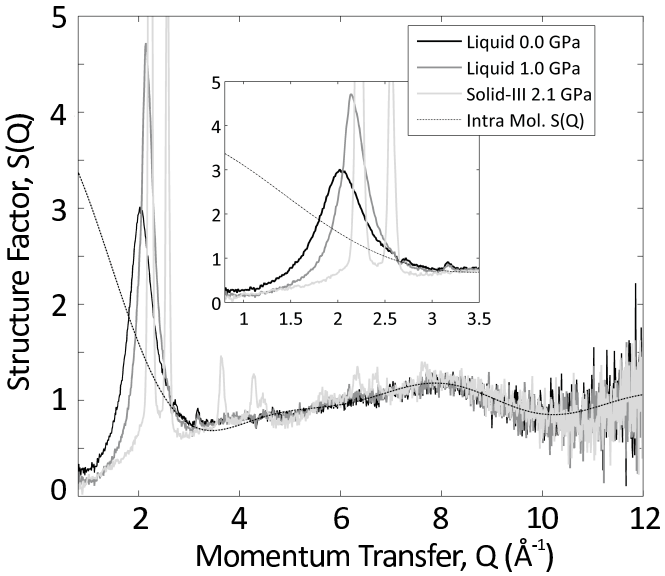

Figure 5 BMR1184B 23FEB2012

Figure 6 Guthrie et al, PRB

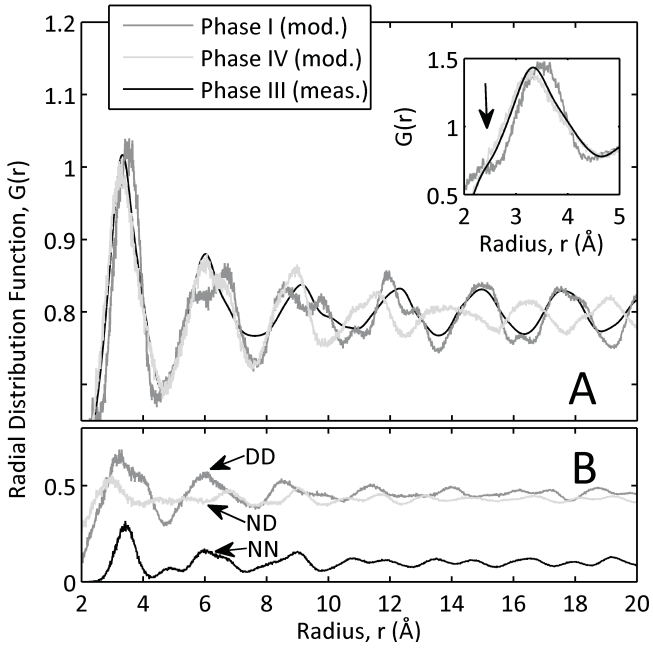

Figure 6 BMR1184B 23FEB2012

Figure 7 Guthrie et al, PRB

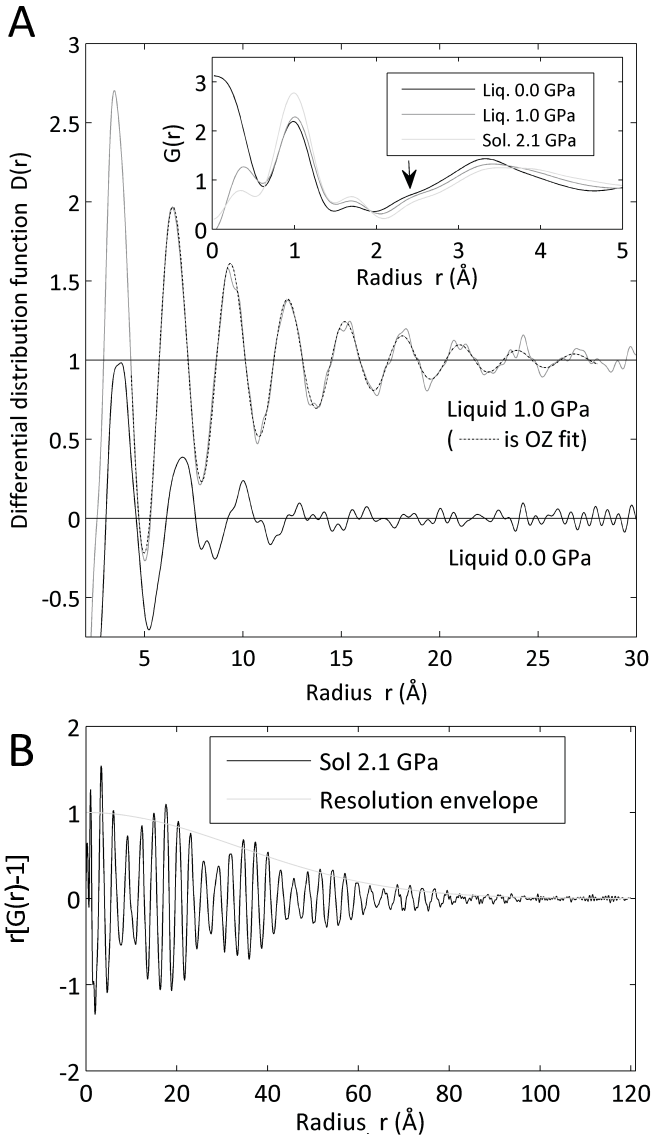

Figure 7 BMR1184B 23FEB2012